ISSN 0016-7932, Geomagnetism and Aeronomy, 2022, Vol. 62, No. 1, pp. 134–142. © Pleiades Publishing, Ltd., 2022.

Spitze Angle Changes during Rapid Geomagnetic Core Field Variation

A. G. Elias[a, b, *], M. Fagre[c, d, *], B. S. Zossi[a, b, **], and H. Amit[e, ****]**

[a] *LIANM, Departamento de Física, Facultad de Ciencias Exactas y Tecnología, Universidad Nacional de Tucuman, Tucumán, 4000 Argentina*

[b] *INFINOA (CONICET-UNT), Tucuman, 4000 Argentina*

[c] *Consejo Nacional de Investigaciones Científicas y Técnicas, CONICET, Argentina*

[d] *Laboratorio de Telecomunicaciones, Departamento de Electricidad, Electrónica y Computación, Facultad de Ciencias Exactas y Tecnología, Universidad Nacional de Tucuman, Tucuman, 4000 Argentina*

[e] *Laboratoire de Planétologie et de Géodynamique, CNRS, Université de Nantes, Nantes, 44322 France*

**e-mail: aelias@herrera.unt.edu.ar*

***e-mail: bzossi@herrera.unt.edu.ar*

****e-mail mfagre@herrera.unt.edu.ar*

*****e-mail Hagay.Amit@univ-nantes.fr*

Received December 14, 2020; revised June 18, 2021; accepted September 24, 2021

Abstract—The spitze phenomenon is an outstanding feature of electromagnetic wave propagation through the ionosphere. It consists in a ray path cusp that occurs between vertical propagation and a critical angle called the spitze angle. This angle that depends on the propagating wave frequency and on the geomagnetic field intensity and inclination, has gained renewed importance for its role in ionospheric modification by powerful radio wave experiments. Here we consider Earth's magnetic field secular variation on two distinctive timescales. First, the most drastic scenario considered is a polarity reversal. We present consequent changes in the spitze angle for three plausible transitional scenarios. Second, we track changes during the past 115 years based on geomagnetic field observations. Globally, we find that the spitze spatial variation is determined mainly by geomagnetic inclination with larger values for smaller inclinations. However, locally the spitze time variation differs from site to site and may depend on the evolution of either field intensity or inclination. Despite the long-term timescales considered, understanding the origin of the spitze spatio-temporal variations on various timescales is important from a physical point of view to unravel magnetized plasma phenomena.

DOI: 10.1134/S0016793222010066

1. INTRODUCTION

Radio waves with a frequency range of 3–30 MHz, designated as high frequency (HF) waves, are used in long-distance communication and detection. Some outstanding features of radio wave propagation in the ionospheric plasma, such as the spitze phenomenon, bi-refraction, the existence of radio windows and some special effects when the frequency of a radar transmitter is close to a harmonic of the electron gyrofrequency, are controlled by the Earth's magnetic field. In particular, the spitze phenomenon (Poeverlein, 1948) occurs for the ordinary ray when the propagation is in the magnetic meridian for incident angles in the range between zero (vertical incidence) and a critical value called spitze angle, ϕ_c. This angle depends on the propagating wave frequency, f, and on the geomagnetic field intensity and inclination, B and I respectively (Davies, 1965). The importance of the spitze angle concept received increasing interest due to its application in ionospheric modification by powerful radio wave experiments and ionospheric heating (Isham et al., 2005; Honary et al., 2011; Liu et al., 2018; Streltsov et al., 2018) since it corresponds, together with the magnetic zenith, to limits for obtaining the maximum topside backscattered power.

The incidence angle of the ordinary mode (O-mode) within the spitze results in a Z-mode (which corresponds to a slow extraordinary mode) conversion process. The Z-mode is able to penetrate to altitudes above the O-mode reflection height, where the conversion of electromagnetic waves to electrostatic waves, or plasma modes, is more efficient, inducing Langmuir waves and excitation of upper hybrid resonance oscillations. Theoretically, this leads to a more rapid development of the resonance instability and potentially a greater magnitude of electron temperature enhancement. The spitze angle value defines then an angle range between ± this

value, called Z-mode window or Ellis-window (Ellis, 1953, 1955, 1956; Smith, 1973), for which mode conversion from the initial ordinary wave to an extraordinary polarized Z-mode wave is favorable (Mjølus, 1984, 1990; Mishin et al., 2016). The coupling between these modes is more efficient when the incident angle coincides with the Spitze angle (Kim and Lee, 2006). Numerical simulations obtain the enhanced O-mode to Z-mode conversion at the Spitze direction (Cannon, 2016; Cannon et al., 2016).

This situation changes at low latitudes, as shown by Eliasson and Papadopoulos (2016), who analyzed the propagation and non-linear interaction between large-amplitude electromagnetic waves and the ionospheric plasma in the magnetic equatorial region, where the magnetic field is dominantly horizontal. Here, O-mode waves injected vertically and within the spitze region lead to the excitation of artificial ionospheric turbulence. In addition, there are HF heating experiments at Arecibo, where the beam is directed vertically while the inclination of the geomagnetic field is 43.5° (Eliasson et al., 2018).

In general, even though the strongest effects on the ionospheric plasma occur when the radar angle is close to the magnetic zenith angle, the spitze angle also plays a role. For example, Watanabe et al. (2014) showed an enhancement of the parametric decay, through strong Langmuir turbulence generation, with the HF pointing angle between the spitze angle and the magnetic zenith angle. The role of the spitze angle within experiments is also mentioned by Eliasson et al. (2015) and Mishin et al. (2016). So, even though it is not the optimum angle for artificial ionospheric heating experiments, it acts as a limit, especially within theoretical studies.

The Earth's magnetic field, key to the spitze effect, varies greatly with time. Over millennial timescales, the most drastic change occurs during polarity reversals. In the past 5 million years, reversals took place every ~200000 years on average, although this frequency is highly variable (Jacobs, 1994; Glassmeier et al., 2009; Olson and Amit, 2015). In fact, the last reversal occurred about 780000 years ago (Jacobs, 1994). During a polarity reversal, which lasts between ~2000 and 12000 years (Clement, 2004), the field at the Earth's surface may diminish to about 10% of its normal magnitude and may also substantially change its configuration. The present field can be approximated by a geocentric magnetic dipole with its axis tilted ~10° with respect to Earth's rotational axis. This dipole accounts for ~80% of the magnetic field power at the Earth's surface while non-dipolar components make for the remaining ~20%. On decadal timescales, since the advent of geomagnetic intensity measurements the axial dipole has been rapidly decreasing (e.g. Olson and Amit, 2006; Finlay, 2008).

Although the understanding of geomagnetic reversals has improved considerably over the years (e.g. Valet and Fournier, 2016), the dominance of a dipolar or multi-polar configuration during polarity transitions is still under debate. Amit et al. (2010) summarized several reversal scenarios with two extremes for the dipolar component: a dipole collapse and a dipole rotation where only the axial dipole would vanish by transferring its energy to the equatorial dipole components. Regarding the non-dipolar field, Amit et al. (2010) considered three main possibilities: (1) decrease and recovery in phase with the dipole collapse, (2) remains unchanged, or (3) grows throughout the reversal possibly due to energy transfer from the dipole (Amit and Olson, 2010; Huguet and Amit, 2012) or dynamo configurations favouring the generation of a non-dipolar field.

Variations in Earth's magnetic field strength and morphology can impact several aspects of ionospheric physics (which includes basically space plasma physics and magnetohydrodynamics) such as radio wave propagation, thermosphere-ionosphere dynamics, and space weather. However, the field's secular variation consequences on radio wave propagation with a paleomagnetic perspective were barely studied (Fagre et al., 2020). In the present work the spitze angle variation is determined for three plausible geomagnetic field configurations during reversals. Although these reversal scenarios are hypothetical, they may encompass some key ingredients of paleomagnetic reversals (Amit et al., 2010). These scenarios were recently considered to study variations in ionospheric Hall and Pedersen conductances (Zossi et al., 2018), in the location and shape of polar caps (Zossi et al., 2019) and some effects on radio wave propagation (Fagre et al., 2020). In addition, we explore the spitze angle variation over the past 115 years using the historical geomagnetic field record. Although this short period exhibits far smaller secular variation, the rapid decrease in the geomagnetic dipole intensity during the historical era (e.g. Finlay, 2008) may provide a detectable signature on the ionospheric dynamics (Tsyganenko, 2019; Zossi et al., 2020). Overall, understanding the origin of spitze angle spatio-temporal variations on various timescales is an interesting topic from a geophysical point of view, linked to magnetized plasma phenomena, as well as for its potential practical applications. For example, in combination with the magnetic zenith angle, changes in the spitze angle may provide insight to the direction (elevation and azimuth) of the HF signal used to pump the ionosphere.

The theoretical background of our study is described in section 2 followed by the methodology in section 3. Results are presented in section 4, and some concluding remarks are discussed in section 5.

2. THEORY

The spitze phenomenon was discovered by Hermann Poeverlein in 1948 (Poeverlein, 1948; Davies, 1965). It consists in a discontinuity or cusp at the reflec-

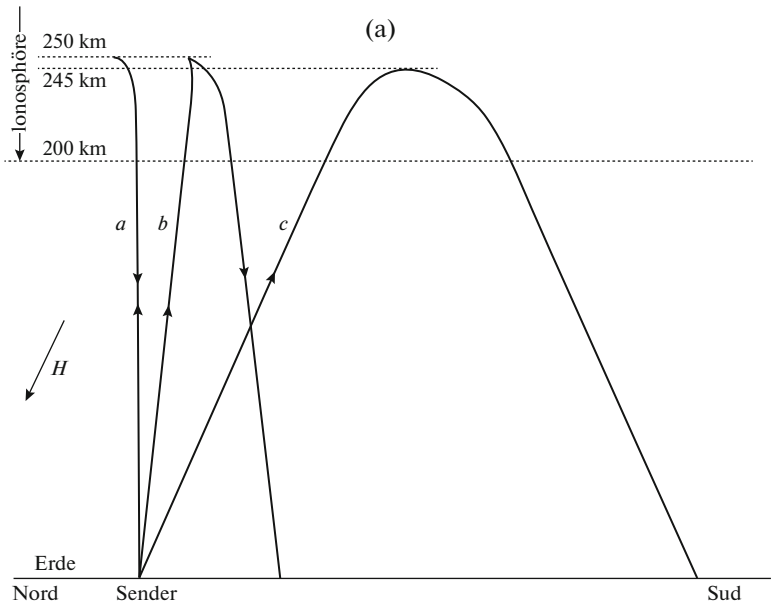

Abb. 3. Strahlwege des ordentlichen Strahls (Daten S. 187)
H = Richtung des Erdmagnefelds

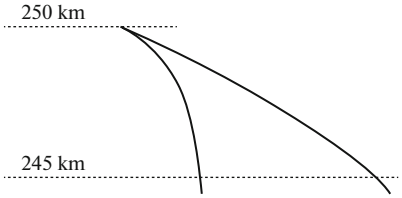

Zu Abb. 3. Vergrößerte Darsellung der Spitze von Strahlweg *b*

Fig. 1. Schematic illustration of the sptize angle ϕ_c shown from Fig. 3 of the original paper by Poeverlein (1948). (a) Ordinary ray paths for increasing incident angle ϕ: *a* corresponds to $\phi = 0$, *b* to $\phi < \phi_c$, and *c* to $\phi > \phi_c$. Only rays *a* and *b* show a spitze. (b) Enlarged view of the "spitze" of the ray path. (Permission to reproduce the illustration granted by Bayerische Akademie der Wissenschaften).

tion point in some ray paths of an electromagnetic wave travelling through the ionospheric plasma. This ray path cusp is called "spitze", a term adapted from German (meaning "pointed" or "sharp"). Figure 1 shows a schematic illustration of the spitze phenomenon obtained from the original paper by Poeverlein (1948). To introduce the concept of the spitze angle, intimately related to this phenomenon, we present the following explanation.

Considering the neutral atmosphere below the ionosphere as a free space with refractive index $n = 1$, an electromagnetic wave travelling from below and entering the ionosphere is refracted along its path due to n variation. Ionospheric n, assuming a cold magnetoplasma where only electrons need to be taken into account (valid approximation for the propagation of HF signals in the ionosphere), is given by the Appleton-Hartree equation, that is

$$n = \sqrt{1 - \frac{2X(1-X)}{2(1-X) - Y^2\sin^2(\Theta) \pm \sqrt{Y^4\sin^4(\Theta) + 4(1-X)^2 Y^2\cos^2(\Theta)}}}, \quad (1)$$

with

$$X = \frac{f_o^2}{f^2} = \frac{Ne^2}{m\varepsilon_o(2\pi f)^2}, \quad (2)$$

$$Y = \frac{f_B}{f} = \frac{eB}{m2\pi f}, \quad (3)$$

where f_o is the plasma frequency, f_B the gyrofrequency, N the electron number density, e the electron charge,

m the electron mass, ε_o the free space permittivity, and the angle Θ corresponds to the angle between the direction of the wave propagation and the magnetic field vector. The upper sign in the denominator refers to the ordinary and the lower sign to the extraordinary components respectively, which result from double refractivity of the ionosphere due to the Earth's magnetic field presence.

When a radio wave has vertical incidence at the base of the ionosphere, that is $\phi = 0$, it reflects from the height level where $X = 1$, that is when n becomes 0 (or equivalently when f reaches f_o) independent of the magnetic field value or orientation. As the incidence angle increases, when it travels in the magnetic meridian, it still reflects from the same height level where $X = 1$, up to an upper critical incidence angle ϕ_c, called spitze angle, that corresponds to (Poeverlein, 1948; Budden, 1960)

$$\sin(\phi_c) = \sqrt{\frac{Y}{1+Y}}\cos(I), \tag{4}$$

where the wave normal becomes parallel to the magnetic field.

This expression is obtained considering the Booker quartic equation as done by Budden (1960) or from Poeverlein's graphical method (Poeverlein, 1948). It can also be deduced with the following considerations, knowing "a priori" the propagation conditions. If the incident angle at the base of the ionosphere is ϕ_c where $n = 1$, the angle of the wave normal at the reflection point will be I, since, according to these propagation conditions (Poeverlein, 1948; Budden, 1960) it becomes parallel to the geomagnetic field. The angle of refraction is then (90-I) and $\Theta = 0$. According to Snell's law $\sin(\phi_c) = n\cos(I)$. Substituting $\Theta = 0$ in Equation (1), considering the + sign for the ordinary mode, and then substituting $X = 1$, gives at the reflection point $n = (Y/1 + Y)^{1/2}$, which is consistent with Snell's law in Equation (4).

For greater ϕ values the wave reflects at lower heights. That is, for $0 \le \phi \le \phi_c$ and a given f, the wave reaches the highest possible level for that frequency, corresponding to $X = 1$. In doing this, the ordinary wave ray path never becomes horizontal, as mentioned at the beginning of this section, and n takes suddenly the value corresponding to reflection conditions producing the discontinuity or cusp in the ray path called "spitze".

According to Equation (4), ϕ_c depends on two factors: Y and cos(I). The first factor, Y, corresponds to the f_B/f ratio that depends on B and f, as seen in Equation (3). Within the HF range, f has a sub-range of possible values within which the radio wave can be reflected. It goes from a lower limit imposed by f_o values at the ionospheric E-layer (not much smaller than its critical value foE ~ 3–4 MHz), to a maximum value, which for almost perpendicular incidence as our case, does not exceed much the $F2$-layer critical frequency $foF2$ (~8–10 MHz). This puts an upper limit to Y corresponding to the maximum possible B (which for the present field corresponds to ~65000 nT) and the minimum possible f, which implies $Y \sim 0.4$. Combining with the maximum cos(I) value, that is 1, we obtain a maximum hypothetical ϕ_c of ~32°. In practice this value is not reached because in the present almost dipolar field, maximum cos(I) takes place at the minimum B, hence the maximum attainable ϕ_c is lower being ~28°. These limits on Y, which varies between 0 and ~0.4, turn the cos(I) factor running from 0 to 1 into the more determinant factor of ϕ_c spatial variation.

3. METHODOLOGY

The spatial variation of the spitze angle was assessed on a 1° × 1° latitude-longitude grid for two applications. First, we considered synthetic reversal scenarios. We calculated the spatial variation of the spitze angle for the present field and three plausible transitional scenarios: an axial dipole collapse where the axial dipolar component is set to zero keeping the equatorial dipole as well as higher degrees unchanged, a dipole rotation transferring the power of the axial dipole on the core-mantle boundary (CMB) to the equatorial dipolar components, and an energy cascade with a transfer of the dipole power on the CMB to the quadrupolar and octupolar components. Second, we considered the observed geomagnetic field in the period 1900–2015 from the International Geomagnetic Reference Field 12th Generation (IGRF12) (Thébault et al., 2015).

The present-day geomagnetic B and I, which are the primary variables needed to calculate ϕ_c, are obtained from IGRF12. For the transitional scenarios we modified accordingly the Gauss coefficients in IGRF12 for 2015. The calculation of these synthetic transitional magnetic field models is described in detail in Zossi et al. (2019).

For the historical time variation, between 1900–2015, we considered the IGRF12 model expanded until spherical harmonic degree and order 13 and in steps of 5-years.

4. RESULTS

Figure 2 shows the spitze angle ϕ_c spatial variation for the present geomagnetic field and for each of the three reversing scenarios. For comparison, Fig. 3 shows the corresponding distributions of cos(I). Largest ϕ_c values occur in regions where cos(I) is largest. For the present field with a dominant axial dipolar configuration, this occurs around the magnetic equator, as seen in Figs. 2a and 3a. Under a dipole rotation scenario the largest ϕ_c also occurs along the corresponding magnetic equator, which in this case is

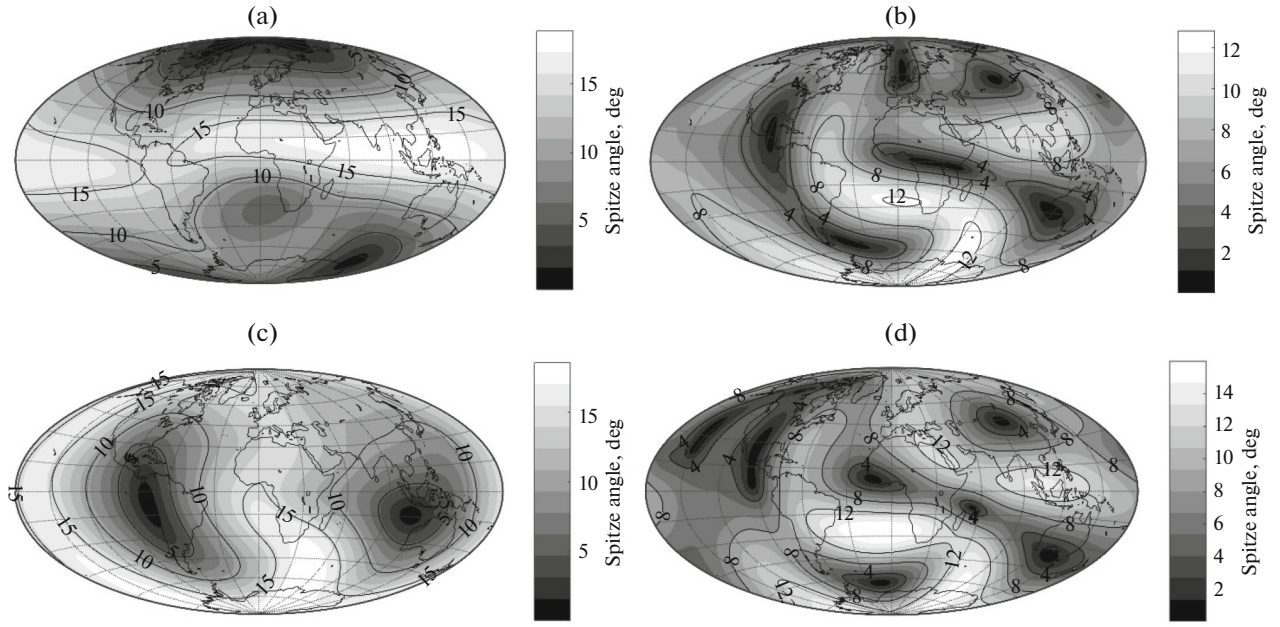

Fig. 2. Spitze angle ϕ_c for $f = 10$ MHz and (a) the present Earth's magnetic field, (b) an axial dipole collapse, (c) a dipole rotation, and (d) an energy cascade. Note the different scales.

almost parallel to a meridian, as noticed in Figs. 2c and 3c. For less dipolar configurations the spitze spatial variability becomes smaller scale with greater ϕ_c at locations with larger cos(I), that is more horizontal field lines, as seen from the comparison of Figs. 2b, 2d with Figs. 3b, 3d. Despite these smaller scale configurations the largest ϕ_c emerge at the southern hemisphere (Figs. 2b, 2d) where the present-day field is less dipolar (e.g. Olson and Amit, 2006).

Minimal ϕ_c occur for more vertical field lines, as is the case at the polar caps. In fact, some of their locations coincide with the polar caps shown in Zossi et al. (2019). There are additional low ϕ_c areas for vertical field line regions which do not correspond to polar caps. For the present-day field smallest ϕ_c appear at the four high-latitude intense geomagnetic flux patches (e.g. Jackson et al., 2000; Amit et al., 2011; Gillet et al., 2015) where the inclination is largest. Also note a relatively small ϕ_c at the South Atlantic Anomaly (Terra-Nova et al., 2017) where the field exhibits strong deviation from dipolarity and relatively large inclination (Figs. 2a and 3a). Overall, for all four field configurations the two quantities ϕ_c and cos(I) exhibit high spatial correlation, as expected.

The spatial variation of ϕ_c due to the secular geomagnetic field variation in the last 115 years is much smaller than that predicted for reversal scenarios, to the point that it is almost identical to that shown in Fig. 2a. However, even small, we can analyse in this case the time variation for two locations that are extreme cases: (8° N, 96° E) which presents the largest ϕ_c value (18.8° considering $f = 10$) for 2015, and (86° N, 153° W) which presents a very low ϕ_c value (0.03° again considering $f = 10$). Figure 4 shows ϕ_c time evolution during the last 115 years for these selected locations. Calculations were performed every 5 years beginning in 1900. Here, B and cos(I) are also plotted to show how the ϕ_c time variation in one of the selected locations follows very closely B (and not cos(I)), and in the other it follows very closely cos(I) (and not B). At low latitudes the inclination is small (or cos(I) is large, see Fig. 3a) so the local intensity exhibits relatively larger temporal variability and hence dominates the evolution of the ϕ_c value (Fig. 4a), whereas at high latitudes the inclination is large (Fig. 3a) so relatively large temporal changes in cos(I) dominate the evolution of the ϕ_c value (Fig. 4d).

As an application of our study, Fig. 5 presents ϕ_c time evolution for two locations which have high-power transmitters for ionospheric studies and consider the spitze angle value for their experiments: Gakona (62° N, 145° W), Alaska, and Tromso (70° N, 19° E), Norway. These two sites belong to The High-frequency Active Auroral Research Program (HAARP) (Pedersen et al., 2010) and European Incoherent Scatter (EISCAT) (Rietveld et al., 2016) heating facilities, respectively. Both sites reside at high latitudes where ϕ_c is quite small.

During the historical era the ϕ_c value in Tromso has mostly been decreasing (Figs. 5c, 5d), in agreement with the evolution of the high-latitude weak ϕ_c value site in Fig. 4d. However, the ϕ_c value in Gakona exhibits a more complex evolution with a non-trivial

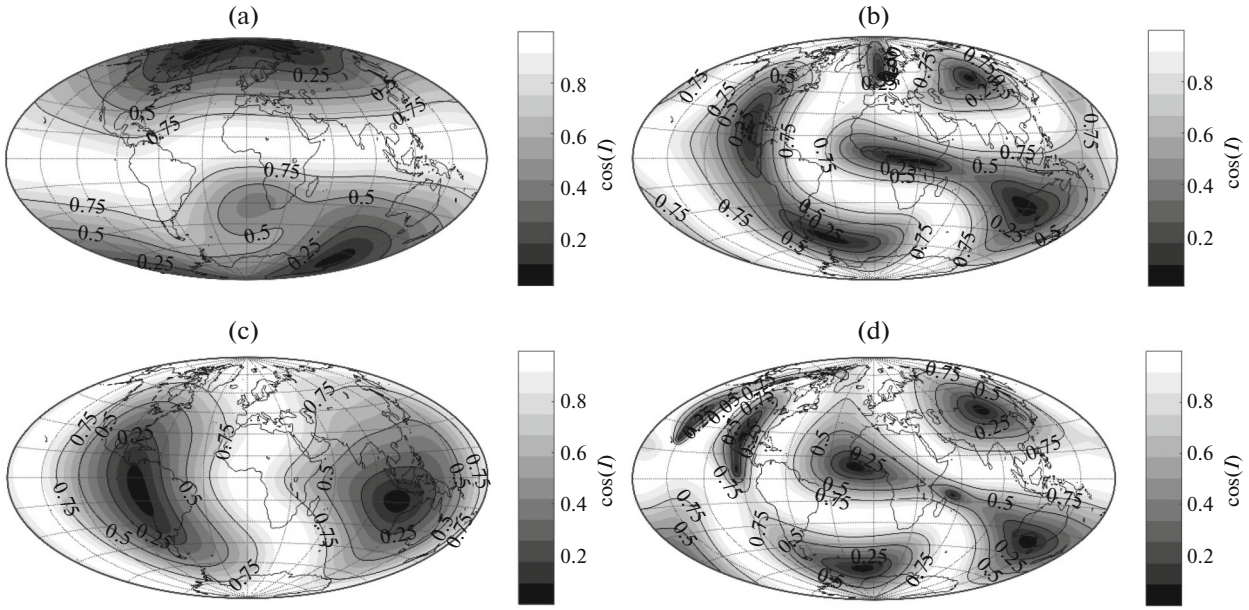

Fig. 3. Inclination angle cosine, cos(*I*), for (a) the present Earth's magnetic field, (b) an axial dipole collapse, (c) a dipole rotation, and (d) an energy cascade.

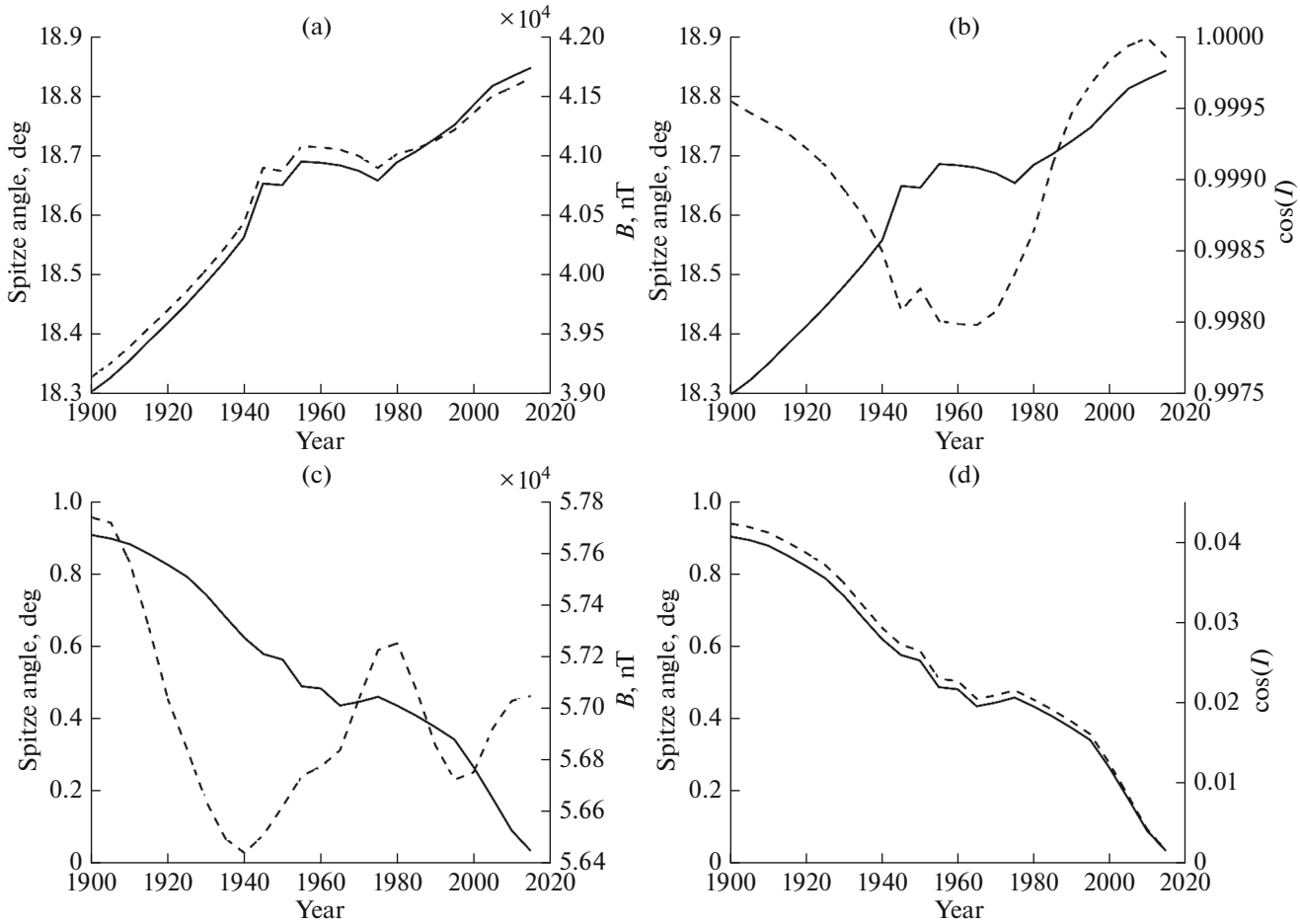

Fig. 4. Spitze angle (solid lines) at (8° N, 96° E) (a)–(b) and at (86° N, 153° W) (c)–(d) together with *B* (dashed lines) in (a)–(c) and cos(*I*) (dashed lines) in (b)–(d) for 1900–2015 based on IGRF12 every 5 years.

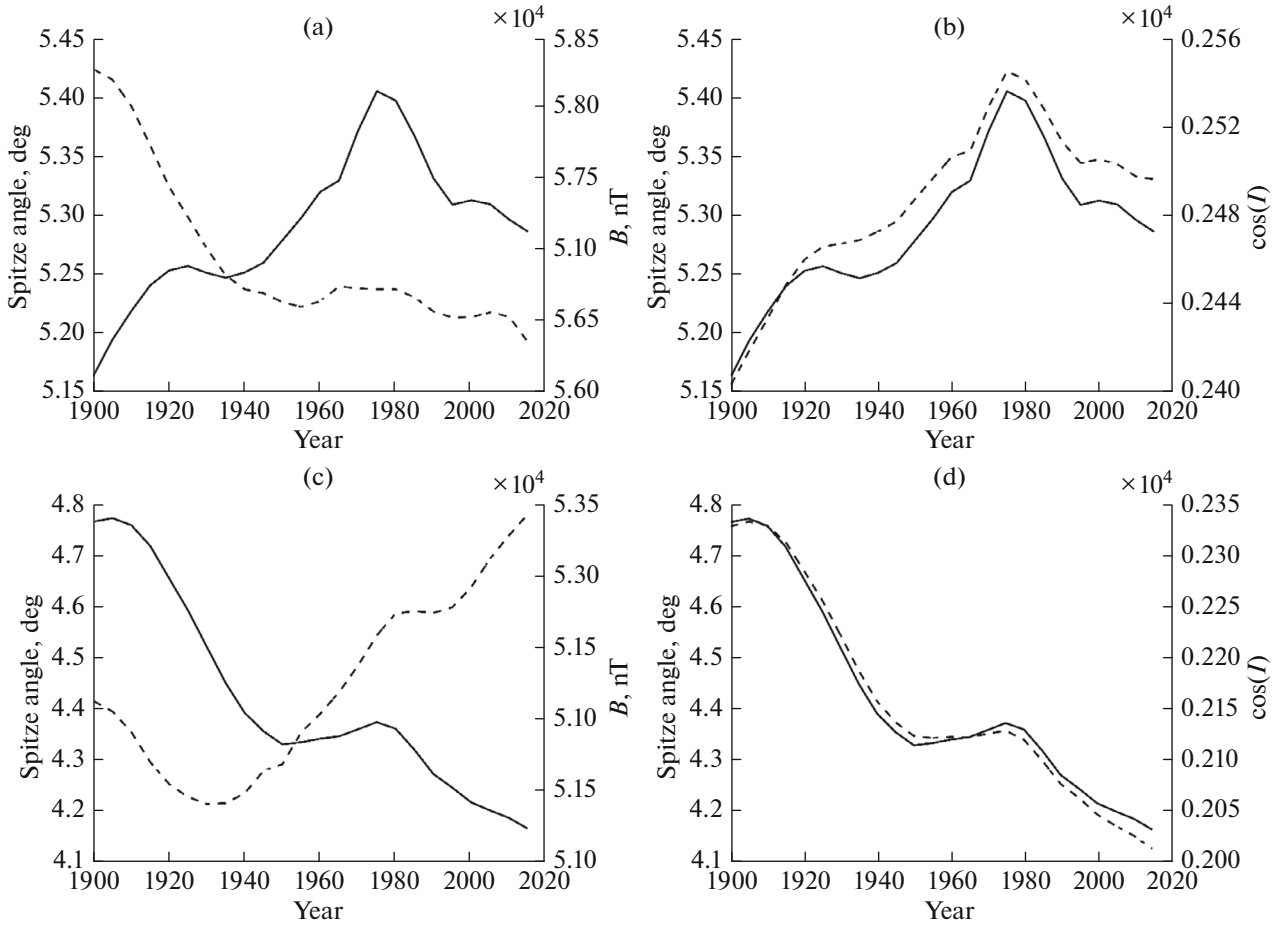

Fig. 5. As in Fig. 4 for Gakona (62° N, 145° W) (a) and Tromso (70° N, 19° E) (b).

increase until ~1980 and a decrease thereafter (Figs. 5a, 5b). In both sites the ϕ_c evolutions follow closely the evolutions of cos(*I*) (Figs. 5b, 5d). Also shown in Figs. 5a, 5c are the B variations at both sites, which differ markedly from that of ϕ_c in these cases at most times.

5. CONCLUSIONS

The spitze angle, which exists only in a magnetized plasma, changes its spatial distribution and time variability according to Earth's magnetic field orientation and intensity. Overall, regions of large or small spitze values are associated with low or high inclination, respectively. For the present field configuration, which is dominantly axial dipolar, the greatest spitze values are found at the magnetic equator, and the lowest at the polar caps. A similar situation occurs for a prevailing equatorial dipole (dipole rotation scenario) at the corresponding magnetic equator, which in this scenario runs through the longitudes of Africa and the mid-Pacific Ocean. For less dipolar transitional field configurations the spitze spatial variability becomes smaller scale, though largest values are found in the southern hemisphere.

Local ϕ_c time variation depends on the relative variation of B and I at each site, which may differ markedly for different geographical regions. At high-latitude sites low spitze angles (Fig. 2a) that are characterized by large inclinations (Fig. 3a) generally have been decreasing during the past 115 years in conjunction with the corresponding local decreases in cos(*I*) (Figs. 4d and 5d). An exception is the site in Alaska that shows an increase until 1980 followed by a decrease until present (Fig. 5a). Indeed, the intense geomagnetic flux patch on the CMB below north America has been more mobile than other high-latitude flux patches (Amit, 2014), with detectable signature of this mobility at Earth's surface as well (Zossi et al., 2020). Conversely, at low-latitude sites large spitze angles (Fig. 2a) that are characterized by small inclinations (Fig. 3a) have been increasing during the past 115 years in conjunction with the corresponding local increase in B (Fig. 4a).

These changes in the spitze angle may be of practical relevance in the far as well as near future. They

could matter for certain applications linked to plasma physics, such as artificial plasma perturbations which are greatest for angles in a narrow band around the spitze angle or somewhere between the spitze and the magnetic field directions. Changes in the spitze angle then will imply changes in the pumping optimal direction to induce the artificial perturbations. Our results demonstrate that the spitze values at particular relevant sites may vary rapidly over decadal timescales (Fig. 5), including sharp temporal change of trend (Figs. 5a, 5b). Over millennial timescales, particularly during a reversal, these sites may witness changes of as much as ~10 degrees in the spitze angle depending on the transitional field configuration.

As stated in the seminal review paper by Yeh and Liu (1972), "one of the most outstanding features of a plasma is the change of its electromagnetic properties when it is under the influence of an external steady magnetic field". This is precisely the case of the ionosphere embedded in Earth's magnetic field, with the spitze phenomenon being one of these outstanding features. Overall, unravelling the electromagnetic properties of the ionospheric plasma during a reversal and in the historical era may highlight possible effects of dipole decrease which is currently ongoing (e.g. Finlay, 2008).

6. ACKNOWLEDGMENTS

We deeply acknowledge Bayerische Akademie der Wissenschaften for granting permission to reproduce Fig. 1 which corresponds to Fig. 3 of Poeverlein, H. (1948), Strahlenwege von Radiowellen in der Ionosphare, Sitzungsberichte der mathematisch-naturwissenschaftlichen Klasse, 78, 175–201. This work was supported by Projects PICT 2018-04447, PIUNT E642 and PIP 294/14 (CONICET).

REFERENCES

Amit, H., Can downwelling at the top of the Earth's core be detected in the geomagnetic secular variation?, *Phys. Earth Planet. Inter.*, 2014, vol. 229, pp. 110–221.

Amit, H. and Olson, P., A dynamo cascade interpretation of the geomagnetic dipole decrease, *Geophys. J. Int.*, 2010, vol. 181, no. 3, pp. 1411–1427.

Amit, H., Korte, M., Aubert, J., Constable, C., and Hulot, G., The time-dependence of intense archeomagnetic flux patches, *J. Geophys. Res.*, 2011, vol. 116, no. 2, pp. 691–704. https://doi.org/10.1002/2014JB011742

Amit, H., Leonhardt, R., and Wicht, J., Polarity reversals from paleomagnetic observations and numerical dynamos simulations, *Space Sci. Rev.*, 2010, vol. 155, pp. 293–335.

Budden, K.G., *Radio Waves in the Ionosphere*, London: Cambridge University Press, 1960.

Cannon, P.D., Numerical simulation of wave-plasma interactions in the ionosphere, *PhD Thesis*, Lancaster University, 2016. https://eprints.lancs.ac.uk/id/eprint/80076/1/2016cannonphd.pdf.

Cannon, P.D., Honary, F., and Borisov, N., Two-dimensional numerical simulation of O-mode to Z-mode conversion in the ionosphere, *J. Geophys. Res.*, 2016, vol. 121, pp. 2755–2782.

Clement, B.M., Dependence of the duration of geomagnetic polarity reversals on site latitude, *Nature*, 2004, vol. 428, pp. 637–640.

Davies, K., *Ionospheric Radio Propagation*, Washington, DC, US Dept. of Commerce, National Bureau of Standards, 1965.

Eliasson, B. and Papadopoulos, K., HF wave propagation and induced ionospheric turbulence in the magnetic equatorial region, *J. Geophys. Res.*, 2016, vol. 121, pp. 2727–2742.

Eliasson, B., Milikh, G., Shao, X., Mishin, E.V., and Papadopoulos, K., Incidence angle dependence of Langmuir turbulence and artificial ionospheric layers driven by high-power HF-heating, *J. Plasma Phys.*, 2015, vol. 81, no. 2, p. 415810201. https://doi.org/10.1017/S0022377814000968

Eliasson, B., Milikh, G.M., Liu, T.C., Shao, X., and Papadopoulos, K., Simulations of the generation of energetic electrons and the formation of descending artificial plasma layers during HF heating at Arecibo, *J. Geophys. Res.*, 2018, vol. 123, pp. 10301–10309.

Ellis, G.R., *F*-region triple splitting, *J. Atmos. Terr. Phys.*, 1953, vol. 3, pp. 263–269.

Ellis, G.R., The magneto-ionic triple splitting of ionospheric echoes, *PhD Thesis*, University of Tasmania, 1955. https://eprints.utas.edu.au/19968/1/whole_ElisGraemeReadeAnthony1955_thesis.pdf.

Ellis, G.R., The z propagation hole in the ionosphere, *J. Atmos. Terr. Phys.*, 1956, vol. 8, pp. 43–54.

Fagre, M., Zossi, B.S., Yigit, E., Amit, H., and Elias, A.G., High frequency sky wave propagation during geomagnetic field reversals, *Stud. Geophys. Geod.*, 2020, vol. 64, pp. 130–142.

Finlay, C., Historical variation of the geomagnetic axial dipole, *Phys. Earth Planet. Inter.*, 2008, vol. 170, pp. 1–14.

Gillet, N., Barrois, O., and Finlay, C.C., Stochastic forecasting of the geomagnetic field from the COV-OBS.x1 geomagnetic field model, and candidate models for IGRF-12, *Earth Plan. Space*, 2015, vol. 67, p. 71. https://doi.org/10.1186/s40623-015-0225-z

Glassmeier, K.H., Soffel, H., and Negendank, J.F.W., *Geomagnetic Field Variations*, Berlin: Springer, 2009.

Honary, F., Borisov, N., Beharrell, M., and Senior, A., Temporal development of the magnetic zenith effect, *J. Geophys. Res.*, 2011, vol. 116. https://doi.org/10.1029/2010JA016029

Huguet, L. and Amit, H., Magnetic energy transfer at the top of Earth's core, *Geophys. J. Int.*, 2012, vol. 190, pp. 856–870.

Isham, B., Hagfors, T., Khudukon, B.Z., Yurik, Y., Tereshchenko, E.D., Rietveld, M.T., Belyey, V., Grill, M., La Hoz, C., Brekke, A., and Heinselman, C., An interferometer experiment to explore the aspect angle dependence of stimulated electromagnetic emission spectra, *Ann. Geophys.*, 2005, vol. 23, pp. 55–74.

Jacobs, J.A., *Reversals of the Earth's Magnetic Field*, Cambridge: Cambridge Univ. Press, 1994.

Kim, K. and Lee, D.H., Invariant imbedding theory of mode conversion in inhomogeneous plasmas. II. Mode conversion in cold, magnetized plasmas with perpendicular inhomogeneity, *Phys. Plasmas*, 2006, vol. 13, p. 042103. https://doi.org/10.1063/1.2186529

Liu, M., Zhou, C., Wang, X., Ni, B.B., and Zhao, Z., Numerical simulation of oblique ionospheric heating by powerful radio waves, *Ann. Geophys.*, 2018, vol. 36, pp. 855–866.

Mishin, E., Watkins, B., Lehtinen, N., Eliasson, B., Pedersen, T., and Grach, S., Artificial ionospheric layers driven by high-frequency radiowaves: An assessment, *J. Geophys. Res.*, 2016, vol. 121, pp. 3497–3524.

Mjølus, E., Coupling to Z mode near critical angle, *J. Plasma Physics*, 1984, vol. 31, pp. 7–28.

Mjølus, E., On linear conversion in a magnetized plasma, *Radio Sci.*, 1990, vol. 25, pp. 1321–1339.

Olson, P. and Amit, H., Changes in Earth's dipole, *Naturwissenschaften*, 2006, vol. 93.

Olson, P. and Amit, H., Mantle superplumes induce geomagnetic superchrons, *Front. Earth Sci.*, 2015, vol. 3, pp. 519–542.

Pedersen, T., Gustavsson, B., Mishin, E., Kendall, E., Mills, T., Carlson, H.C., and Snyder, A.L., Creation of artificial ionospheric layers using high-power HF waves, *Geophys. Res. Lett.*, 2010, vol. 37. https://doi.org/10.1029/2009GL041895

Poeverlein, H., Strahlenwege von Radiowellen in der Ionosphäre (Ray paths of radio waves in the ionosphere), *Sitzungsber.-Bayer. Akad. Wiss., Math.-Naturwiss. Kl.*, 1948, vol. 78, pp. 175–201.

Rietveld, M.T., Senior, A., Markkanen, J., and Westman, A., New capabilities of the upgraded EISCAT high-power HF facility, *Radio Sci.*, 2016, vol. 51, pp. 1533–1546.

Smith, M., Numerical solution of the "Ellis window" problem, *Nature Phys. Sci.*, 1973, vol. 243, p. 29.

Streltsov, A.V., Berthelier, J.J., Chernyshov, A.A., Frolov, V.L., Honary, F., Kosch, M.J., McCoy, R.P., Mishin, E.V., and Rietveld, M.T., Past, Present and future of active radio frequency experiments, *Space Sci. Rev.*, 2018, vol. 214, p. 118. https://doi.org/10.1007/s11214-018-0549-7

Terra-Nova, F., Amit, H., Hartmann, G.A., Trindade, R.I.F., and Pinheiro, K.J., Relating the South Atlantic Anomaly and geomagnetic flux patches, *Phys. Earth Planet. Inter.*, 2017, vol. 266, pp. 39–53.

Thébault, E., Finlay, C.C., Beggan, C.D., Alken, P., Aubert, J., Barrois, O., Bertrand, F., Bondar, T., Boness, A., Brocco, L., et al., International geomagnetic reference field: The 12th generation, *Earth Planets Space*, 2015, vol. 67, p. 79. https://doi.org/10.1186/s40623-015-0228-9

Tsyganenko, N.A., Secular drift of the auroral ovals: How fast do they actually move? *Geophys. Res. Lett.*, 2019, vol. 46, pp. 3017–3023.

Valet, J.-P. and Fournier, A., Deciphering records of geomagnetic reversals, *Rev. Geophys.*, 2016, vol. 54, pp. 410–446.

Watanabe, N., Golkowski, M., Sheerin, J.P., and Watkins, B.J., Simultaneous multi-angle observations of strong Langmuir turbulence at HAARP, *Earth Moon Planets*, 2015, vol. 116, pp. 89–100.

Yeh, K.C. and Liu, C.H., Propagation and application of waves in the ionosphere, *Rev. Geophys.*, 1972, vol. 10, pp. 631–709.

Zossi, B.S., Elias, A.G., and Fagre, M., Ionospheric conductance spatial distribution during geomagnetic field reversals, *J. Geophys. Res.*, 2018, vol. 123, pp. 2379–2397.

Zossi, B.S., Fagre, M., Amit, H., and Elias, A.G., Polar caps during geomagnetic polarity reversals, *Geophys. J. Int.*, 2019, vol. 216, pp. 1334–1343.

Zossi, B.S., Fagre, M., Amit, H., and Elias, A.G., Geomagnetic field model indicates shrinking northern auroral oval, *J. Geophys. Res.*, 2020, vol. 125. https://doi.org/10.1029/2019JA027434